ChemPubSoc Europe

DOI: 10.1002/celc.201600518

CHEMELECTROCHEM Articles

One-Dimensional Copper(II) Coordination Polymer as an Electrocatalyst for Water Oxidation

Rupali Mishra,[a] Emine Ülker,[a, b] and Ferdi Karadas*[a, c]

Although cobalt-based heterogeneous catalysts are the central focus in water oxidation research, interest in copper-based water oxidation catalysts has been growing thanks the great abundance of copper and its biological relevance. Several copper oxides have recently been reported to be active catalysts for water oxidation. In this study, a heterogeneous copper-based water oxidation catalyst that is not an oxide has been reported for the first time. Single-crystal XRD studies indicate that the compound is a one-dimensional coordination compound incorporating copper paddle-wheel units connected through phosphine dioxide ligands. The catalyst exhibits an onset potential of 372 mV at pH 10.2, whereas an overpotential of only 563 mV is required to produce a current density of 1 mA cm^{-2}. In addition to cyclic voltammetric and chronoamperometric studies, an investigation into the effect of pH on the catalytic activity and the robustness of the catalyst using long-term bulk electrolysis (12 h) is presented.

1. Introduction

Significant efforts have been devoted to electrocatalytic splitting of water, particularly in the last two decades, to implement hydrogen economy as a renewable and clean alternative to fossil fuels. One of the main challenges in the pursuit of this task is to develop efficient, robust, and inexpensive catalysts for the water oxidation half reaction, which involves a $4H^+/4e^-$ process with relatively high potential [$E = 0.82$ V, pH 7 vs. NHE, 25 °C; Eq. (1)]:

$$2H_2O \rightarrow O_2 + 4H^+ + 4e^- \quad (1)$$

Although oxides of precious metals, such as RuO_2[1] and IrO_2,[2] exhibit high performance in the oxygen evolution reaction, the main focus in this field has been the investigation of compounds incorporating 3d metal ions (particularly Co,[3] Mn,[4] and Ni).[5] Some of the benchmark studies include the cobalt phosphate (Co–Pi) catalyst,[6] cobalt polyoxometalates (Co–POM),[7] [NiO(OH)],[8] and birnessite-type MnO_2.[9]

Recently water oxidation catalysts (WOCs) containing copper have also received attention, as copper is the second most earth-abundant metal and it is biologically relevant considering the key role it has in several oxidation processes such as those involving methane monooxygenase[10] and cytochrome *c* oxidase.[11] The portfolio of WOCs containing copper involves various compounds ranging from homogeneous molecular complexes such as Cu–bipyridine,[12] copper carbonates,[13] and Cu–tetrapeptide[14] systems to three-dimensional heterogeneous copper oxides.[15] In 2012, Mayer et al. reported the first example of a homogeneous copper electrocatalyst for water oxidation with a simple formula of [(bpy)Cu(OH)$_2$] (bpy = 2,2′-bipyridine).[12] Lin et al. later reported that substitution of the bpy ligand with 6,6′-dihydroxy-2,2′-bipyridine leads to a significant increase in the catalytic activity due to ligand oxidation.[16] By contrast, several studies performed on copper oxide systems suggest that copper(II) ions surrounded by oxygen atoms can also electrocatalytically oxidise water.[17] Moreover, the investigation of water oxidation performance of different copper(II) salts in the presence of carbonate or phosphate buffers indicates that the ligands around the metal ion play a key role in the robustness and the catalytic activity of copper ions.[13] Given the aforementioned study, our recent efforts have been concentrated on decorating the coordination sphere of the Cu^{II} site with oxygen groups that belong to acetate and phosphorus-containing ligands, which are stable at anodic potentials. Whereas phosphines are suitable coordinating ligands particularly for low-valent metal ions due to their strong σ-donating ability, phosphine oxides could also be used for coordination to metal sites.[18] Coordination compounds based on dinuclear copper acetate groups, also known as copper paddle-wheel complexes, have been reported previously. Copper-acetate-based coordination polymers have received attention in the fields of magnetism,[19] gas adsorption,[20] and biology[21] mainly due to the stability and structural integrity of paddle-wheel systems.

Our preliminary studies show that copper acetate in aqueous solution exhibits significant catalytic activity at anodic po-

[a] Dr. R. Mishra, Prof. E. Ülker, Prof. F. Karadas
Department of Chemistry, Bilkent University
06800 Ankara (Turkey)
E-mail: karadas@fen.bilkent.edu.tr

[b] Prof. E. Ülker
Department of Chemistry, Faculty of Arts & Sciences
Recep Tayyip Erdogan University, 53100 Rize (Turkey)

[c] Prof. F. Karadas
Institute of Materials Science and Nanotechnology (UNAM)
Bilkent University, 06800 Ankara (Turkey)

Supporting Information and the ORCID identification number(s) for the author(s) of this article can be found under http://dx.doi.org/10.1002/celc.201600518.

tentials (Figure S1 in the Supporting Information). Because heterogeneous catalysts have several advantages over homogeneous catalysts, such as easy implementation and higher stability, our research efforts have recently focused on obtaining heterogeneous WOCs that incorporate copper paddle-wheel groups. In this study, the synthesis, crystal structure, and characterisation of a novel 1D copper(II) coordination polymer, abbreviated as $[Cu_2–P_o]_n$, are reported. Electrochemical and electrocatalytic water oxidation studies performed on fluorine-doped tin oxide (FTO) electrodes coated with the compound, as well as long-term (12 h) catalytic studies and characterisation studies on the pristine and post-catalytic electrodes are also reported in detail.

2. Results and Discussion

2.1. Synthesis and Crystal Structure

The phosphine dioxide ligand used in this study was synthesised by oxidising 1,2-bis(diphenylphosphino)ethane with hydrogen peroxide. The reaction of phosphine dioxide with copper acetate in a methanol/dichloromethane mixture led to the formation of dark blue crystals. The structure of $[Cu_2–P_o]_n$ was successfully solved and converged in the monoclinic space group P121/*n1*. Crystallographic data and structural refinement parameters for the compound are given in Table S1. The crystal structure of $[Cu_2–P_o]_n$ consists of centrosymmetric dimeric molecules with $[Cu_2(\mu\text{-}OAc)_4]$ (OAc = acetate) units linked to each other with 1,2-bis(diphenylphosphino)ethane dioxide (P_o) bridging groups through copper(II) sites (Figure 1). The bridging ligand P_o is connected to copper paddle-wheel units in a monodentate fashion (Figure 2). The asymmetric unit of the crystal structure contains one copper(II) paddle-wheel group with half occupancy and one ligand unit, P_o. The crystal structure of $[Cu_2–P_o]_n$, thus, could best be described as 1D zigzag chains that consists of independent $[Cu_2(\mu\text{-}AcO)_4]$ paddle-wheel units linked by P_o bridging groups. Each metal ion is surrounded by five oxygen atoms, one of which is the oxygen of the phosphine dioxide ligand, whereas the other four belong to acetate bridging groups, thus the complex adopts a square pyramidal coordination environment. In each paddle-wheel unit, the Cu···Cu distance is 2.658 Å. All of the Cu–O distances are within the normal ranges allowing for statistical errors (Table S1).[22] The packing diagram of the compound depicting the arrangement of the 1D chains with respect to each other is shown in Figure S2.

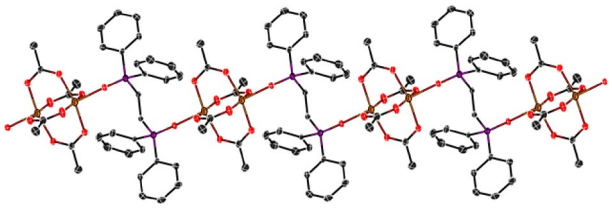

Figure 1. 1D chain structure of $[Cu_2–P_o]_n$. Colour code: Cu = orange; P = purple; O = red; C = grey; N = blue. Thermal ellipsoids are projected at the 50% probability level. Hydrogen atoms are not shown for clarity.

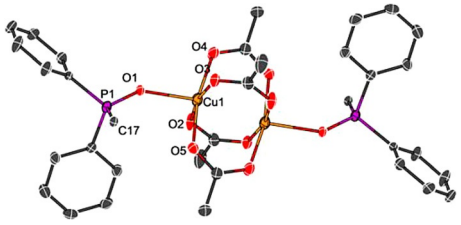

Figure 2. Structure of a segment of the chain in $[Cu_2–P_o]_n$, showing only one copper paddle-wheel unit.

2.2. Electrocatalytic Water Oxidation

Cyclic voltammetry (CV) studies were performed to investigate the electrochemical behaviour of $[Cu_2–P_o]_n$-modified FTO electrodes in KBi solution at different pH values. CV revealed an onset oxidative catalytic current wave, which is attributed to catalytic O_2 evolution, at 1.05 V at pH 9.2 (Figure 3). As the basicity of the medium is increased gradually from pH 9.2 to 12.2 the onset potential of the aforementioned wave shifts from approximately 1.05 to 0.9 V, whereas the current density obtained at 1.5 V (vs. Ag/AgCl) increases from approximately 2 to 6.5 mA cm^{-2}. The plot in Figure 3 (black) that represents the bare FTO electrode shows no appreciable catalytic wave, indicating that the presence of $[Cu_2–P_o]_n$ on the FTO electrode is essential for the catalytic reaction.

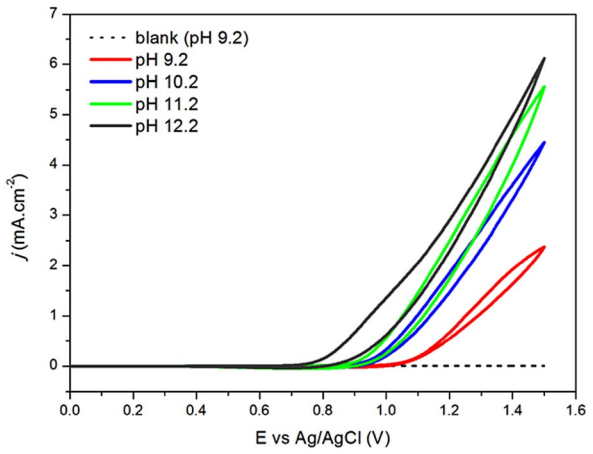

Figure 3. Cyclic voltammograms of the $[Cu_2–P_o]_n$-modified FTO electrode recorded in 0.1 M KBi electrolyte at different pH, recorded at a 50 mV s^{-1} sweep rate. The blank measurement (dashed line) was obtained by using bare FTO as the working electrode.

Chronoamperometric studies were then performed to investigate the catalytic activity of $[Cu_2–P_o]$-modified FTO electrodes in detail. A linear Tafel plot in the range 353–593 mV was obtained at pH 9.2 using KBi as an electrolyte (Figure 4). A slope of 71 mV dec^{-1} was obtained, which suggests a mechanism involving a one-electron chemical pre-equilibrium step that precedes the rate-limiting step.[23] The plot also reveals an onset

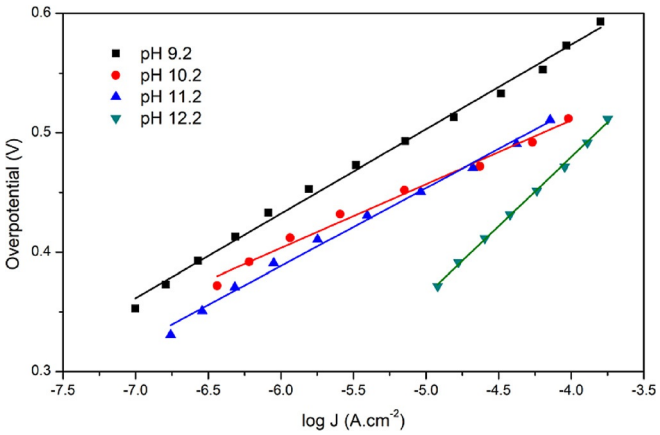

Figure 4. Tafel plots for $[Cu_2–P_o]_n$-modified FTO electrodes obtained at different pH. Ag/AgCl was used as reference electrode and 0.1 M KBi was used as the electrolyte. Tafel slopes of 71, 54, 65, and 116 mV dec^{-1} were obtained at pH values of 9.2, 10.2, 11.2, and 12.2, respectively.

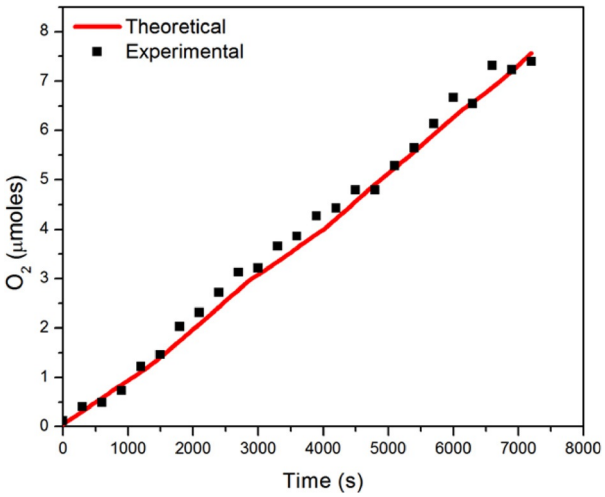

Figure 5. Faradic efficiency of the $[Cu_2–P_o]_n$-modified FTO electrode measured by an oxygen-sensor system. Bulk electrolysis was performed at 1.1 V vs. Ag/AgCl at pH 9.2 in KBi solution in a gas-tight electrochemical cell. The amount of dissolved O_2 molecules detected during bulk electrolysis and the theoretical amount of evolved O_2 assuming a Faradaic efficiency of 100% are represented by the black data points and red line, respectively. A buffer solution of 130 mL was used for experiments. O_2 content was recorded in units of mg L^{-1} and converted to micromoles of O_2.

potential of 353 mV and overpotentials of 644 and 715 mV were required to produce current densities of 1 and 10 mA cm^{-2}, respectively. Chronoamperometric studies were also performed at different pH to investigate the effect of pH on the mechanism of water oxidation. As the pH increases from 9.2 to 11.2, the Tafel slope decreases slightly to approximately 60 mV dec^{-1} and then sharply increases to 116 mV dec^{-1}. This trend suggests that the catalytic oxidation mechanism exhibits similar behaviour at pH 9.2–11.2, whereas the high slope at pH 12.2 could be attributed to a change in the rate-determining step of the water oxidation process. Tafel plots also indicate that the catalyst exhibits the best performance at pH 10.2 with an onset potential of 372 mV and overpotentials of 563 and 617 mV were required to produce current densities of 1 and 10 mA cm^{-2}, respectively. Although the origin of catalytic water oxidation is beyond the scope of this study, the 1D structure implies that copper(II) sites of the paddle-wheel units on the electrode surface, which reside at the end of each chain, that is, the square pyramidal copper(II) sites coordinated to water molecules instead of phosphine dioxide groups, act as oxygen-evolving centres. The catalytic efficiency of the compound is in accordance with previously studied copper-based WOCs (Table S3). Tafel slopes of copper oxides are generally in the range of 54–62 mV dec^{-1}, whereas it is higher for $CuCO_3$,[24] [Bi],[25] O_2–CuCat,[26] and Cu–(TEOA) (TEO = triethanolamine)[27] systems. If the overpotential required for 1 mA cm^{-2} is compared, the catalyst exhibits better performance than CuO(TPA) (TPA = tripropylamine), O_2–CuCat, and Cu–TEOA. The similarity in Tafel slopes between $[Cu_2–P_o]_n$ and copper oxides suggests that the mechanism for water oxidation involves the formation of a peroxide intermediate.[13]

Bulk electrolysis was performed in the presence of an oxygen-sensing probe to monitor the O_2 evolution quantitatively. The amount of O_2 produced during the course of 2 h of electrolysis recorded by the probe and the theoretical amount of evolved O_2 extracted from the total charge are plotted in (Figure 5). The similarities of the two curves clearly indicate that the only origin of current is a catalytic water oxidation process.

Long-term chronoamperometric studies were also performed to investigate the stability of the catalyst. A potential of 1.1 V (vs. Ag/AgCl) was applied for 12 h. The current density was maintained at approximately 270 µA cm^{-2} throughout the measurement, suggesting high durability in the applied conditions (Figure 6). An initial increase in the current density could be attributed to morphological changes on the surface of the electrode similar to those of previously reported copper-based

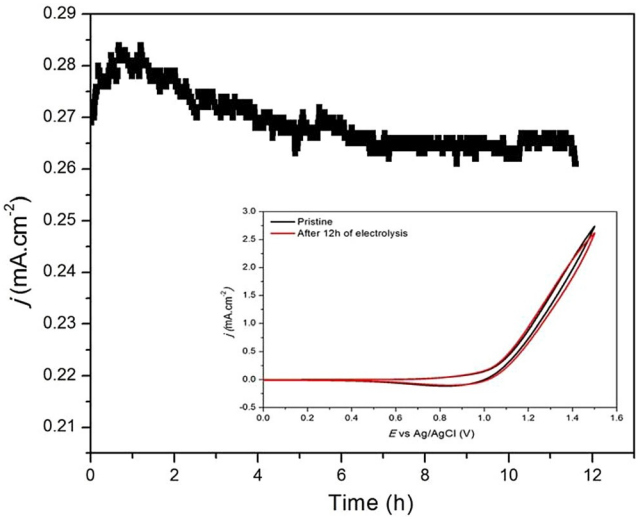

Figure 6. Long-term electrolysis studies for the $[Cu_2–P_o]_n$-modified FTO electrode, performed at 1.1 V (vs. Ag/AgCl) in 0.1 M KBi electrolyte at pH 9.2. Inset: Cyclic voltammograms of the $[Cu_2–P_o]_n$-modified FTO electrode immediately prior to and after 12 h electrolysis.

WOCs.[26] Stability of the electrode was also confirmed by the comparison of cyclic voltammograms of the electrodes recorded before and after electrolysis for 12 h (Figure 6, inset). No significant change in the catalytic current was observed after electrolysis and CV profiles are identical, suggesting high stability of the catalysts (a slight decrease in the peak current can be attributed to the mechanical loss of the catalyst from the surface during catalysis).

2.3. Characterisation

The percentage weight of carbon and hydrogen obtained by elemental analysis of powder sample was in excellent agreement with the molecular formula of the crystal structure, which indicates that the crystal is truly representative of the bulk phase. The chemical integrity of the catalyst deposited on a FTO electrode was investigated with X-ray photoelectron spectroscopy (XPS) and X-ray diffraction (XRD) techniques. XRD patterns of pristine and post-catalytic electrodes (obtained after 2 h of bulk electrolysis at pH 9.2 and 1.1 V vs. Ag/AgCl) were identical and no additional peaks were observed, indicating the chemical integrity of the catalyst during the catalytic process (Figure S4).

XPS survey spectra of both pristine and post-catalytic samples (Figure 7) reveal the catalyst mainly gives Cu 2p, O 1s, C 1s, and P 2p signals, as expected. The high-resolution C 1s spectrum contains a broad signal between 284.2 to 287.4 eV, indicating the presence of carbon in different environments.[28] The P 2p spectrum shows a single peak at 133.3 eV (Figure S5), which can be ascribed to the phosphorus atom of the phosphine oxide ligand.[29] Both the pristine and the post-catalytic samples exhibit broad Cu 2p signals (full width at half-maximum ≈3–6 eV) between 928 and 965 eV that can be attributed to Cu $2p_{3/2}$ and Cu $2p_{1/2}$ peaks, respectively; these correspond to Cu^{2+} species (933.9 and 955.2 eV).[30] Satellite peaks observed at 8–10 eV above the principle peaks support the presence of a partially filled Cu $3d^9$ shell.[26,31] A broad intense peak of O 1s between 530.50 and 534.24 eV can be assigned to different types of oxygen atoms. The peak at 530.7 eV corresponds to the P=O[32] bond, whereas that at around 533.4 eV could be assigned to the C=O of the copper paddle-wheel unit (Figure S4).[33,34] The absence of any scalable shift in the signal positions in the post-catalytic sample suggests that there is no oxide formation on the surface during the catalysis. The Raman spectrum for the Cu compound reveals a CuO_x Ag band at approximately 295 cm^{-1}[35] and a peak at 1700 cm^{-1}, which is the G band of oxygen (Figure S6). The Raman frequencies are consistent with data for pure single-phase CuO_x films having a high degree of crystallinity.

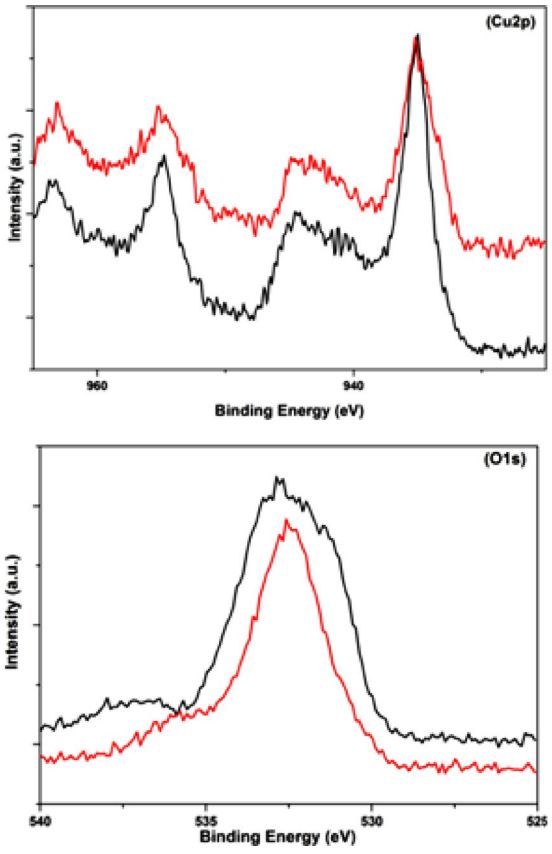

Figure 7. High-resolution XPS spectra of a) Cu 2p and b) O 1s regions for pristine (black) and post-catalytic (red) electrodes.

3. Conclusions

In summary, this study provides a novel example of the use of a copper paddle-wheel system as a heterogeneous WOC. The catalyst required overpotentials of 563 and 617 mV to produce current densities of 1 and 10 mA cm^{-2}, respectively, at pH 10.2. Chronoamperometric measurements were performed also at different pH values to elucidate the mechanism of catalysis. A Tafel slope of approximately 60 mV dec^{-1} at pH 9.2–11.2 suggests a mechanism involving a one-electron chemical pre-equilibrium step preceding the rate-limiting step, and the increase in Tafel slope to 116 mV dec^{-1} at pH 12.2 could be attributed to a change in the rate-determining step of the water oxidation process. The catalyst retained its structure even during 12 h of electrolysis, which was confirmed by XRD, XPS, and Raman techniques, owing to the stability and robustness of the system provided by acetate and phosphine dioxide groups. It is believed that copper(II) sites with square pyramidal geometries on the electrode surface, which are coordinated to water molecules instead of phosphine dioxide ligands, are responsible for the electrocatalytic water oxidation process.

Recently, several copper oxides prepared mainly by the electrolysis of copper(II) salts and complexes in the presence of different electrolytes have been reported to have promising catalytic activities. This study shows that a copper-based coordination compound, rather than an oxide, could also serve as an efficient WOC, and new compounds should be introduced to investigate the ideal coordination sphere for the copper(II) site. Our further studies will focus on new copper paddle-wheel compounds with different coordinating bridging ligands as WOCs to study the effect of such ligands on the surface concentration and, thus, their effect on catalytic activity.

Experimental Section

Materials

1,2-Bis(diphenylphosphino)ethane [1,2-bis(DPPE)], copper acetate monohydrate [$Cu(OAc)_2 \cdot H_2O$], hydrogen peroxide, ethanol, methanol, and dichloromethane were acquired from Sigma–Aldrich and used as received. All solvents were purified prior to use. KBi electrolyte solutions were prepared by mixing approximate volumes of KOH (0.1 M) and H_3BO_3 (0.1 M) with deionised water.

Synthesis of {[Cu_2(μ-OAc)$_4$][1,2-bis(diphenylphosphino)ethane dioxide]}$_n$, [Cu_2–P_o]$_n$

A mixture containing $Cu(OAc)_2 \cdot H_2O$ (0.056 g, 0.3 mmol) and methanol (5 mL) was added to a solution of 1,2-bis(DPPE) (0.056 g, 0.15 mmol) and CH_2Cl_2 (5 mL). The reaction mixture was stirred for 3 h at room temperature and then was added to a solution of methanol (5 mL) and hydrogen peroxide (0.0023 mL, 0.1 mmol). The solution was then stirred for 12 h at room temperature. After filtration, the filtrate was kept at room temperature for slow evaporation. Dark blue-coloured crystals of $[Cu_2–P_o]_n$ were obtained in 78% yield. The crystals were filtered, washed with acetone, and dried in air. Elemental analysis calcd (%) for $C_{17}H_{18}PO_5Cu$: C 51.45, H 4.56; found: C 51.50, H 4.61; IR (ATR): $\tilde{\nu}$ = 1614, 1436, 1196, 1123, 745, 729, 676, 633, 625, 500, 470, 418 cm^{-1} (Figure S3).

Single-Crystal X-ray Diffraction

Single-crystal X-ray data on $[Cu_2–P_o]_n$ was collected at 100 K on a Rigaku MicroMax 007HF diffractometer equipped with a monochromatic MoKα radiation source. The linear absorption coefficients, scattering factors for the atoms, and the anomalous dispersion corrections were taken from the International Tables for X-ray Crystallography.[36] The data integration was performed with SAINT[37] software. An empirical absorption correction was applied to the collected reflections with SADABS[38] and the space group was determined based on systematic absences using XPREP.[39] The structure was solved by the direct methods using SHELXTL-97[40] and refined on F2 by a full-matrix least-squares technique using the SHELXL-97[41] program package. All non-hydrogen atoms were refined anisotropically. The hydrogen atoms attached to carbon atoms were positioned geometrically and treated as riding atoms using SHELXL default parameters. Data collection, lattice parameters and structure solution parameters are collected in Table S1 and selective bond distances and angles are given in Table S2.

Electrochemical Methods

All electrochemical experiments were performed at room temperature and analysed with Gamry Instruments Interface 1000 potentiostat/galvanostat. A conventional three-electrode electrochemical cell was used with Ag/AgCl (3.5 M KCl) as a reference electrode, Pt wire as the counter electrode and FTO (1 × 2 cm; 2 mm slides with 7 Ω sq^{-1} surface resistivity and ≈80% transmittance) as the working electrode. The FTO electrodes were cleaned by sonication in a basic soapy solution, deionised water and isopropanol for 15 min and dried, followed by annealing at 400 °C for 30 min. The catalyst was coated onto a FTO electrode by using a drop-casting method. A mixture of catalyst (5 mg), methanol (1000 μL) and Nafion (100 μL) was sonicated for 30 min. Then, sonicated suspension (50 μL) was dropped onto a clean FTO electrode (1 cm^2). The prepared electrode was dried in an 80 °C oven for 10 min and further used for CV and bulk electrolysis. The electrode was rinsed with deionised water prior to use. All potentials reported in this paper were measured versus the Ag/AgCl reference electrode. Cyclic voltammograms of $[Cu_2–P_o]_n$ coated on FTO were recorded with a scan rate of 50 mV s^{-1} in KBi (0.1 M) electrolyte with different pH values (9.2, 10.2, 11.2 and 12.2) between 0 and 1.5 V (vs. Ag/AgCl).

Bulk Electrolysis

Bulk water electrolysis was performed with a two-compartment cell separated with a glass frit. A Pt wire counter electrode was placed in one compartment and the FTO working electrode and a Ag/AgCl reference electrode were placed in the other. The electrolysis experiments were performed in KBi solution at different pH values. Tafel data were collected under the same conditions at different applied potentials using a steady current density with an equilibrium time of 600 s. Bulk electrolysis was performed at variable potentials without iR compensation.

Faradaic Efficiency and Oxygen Evolution

Oxygen evolution was determined with a YSI 5100 dissolved-oxygen-sensing instrument equipped with a dissolved-oxygen field probe inserted into the anodic compartment. The experiment was performed in a gas-tight electrochemical cell. The electrolyte was degassed by bubbling through high-purity N_2 for 20 min with vigorous stirring. The catalyst coated on a FTO conductive surface was used as the working electrode. The reference electrode was positioned several millimetres from the working electrode. Measurements were recorded at 5 min intervals.

X-ray Photoelectron Spectroscopy

The elemental composition of the catalyst deposited on FTO and the oxidation states of those elements were probed by using a Thermo Scientific K-Alpha X-ray photoelectron spectrometer system operating with an AlKα microfocused monochromator source. The survey scan and the high-resolution Cu 2p spectra were obtained and spectra are referenced to the C 1s peak (285.0 eV).

X-ray Diffraction

The crystal-phase analysis of the sample on the conductive side of FTO before and after bulk electrolysis was measured by XRD patterns were recorded by a Panalytical X'PertPro multipurpose X-ray diffractometer using CuKα radiation (λ = 1.5418 Å). The scanning rate was 5 degree min^{-1} from 20° to 90° in 2θ.

Raman Spectrometry

Raman measurements were performed using a WITEC Alpha 300S system. A diode-pumped solid-state 532 nm wavelength laser was used for excitation. The laser power was calibrated using a silicon photodiode at the sample plane.

Acknowledgements

The authors thank the Scientific and Technological Research Council of Turkey (TÜBİTAK) for financial support (Project No.

214Z095). E.Ü. thanks TÜBİTAK for support (Project 1929B011500059).

Keywords: copper paddle wheel · electrocatalysis · phosphine dioxide · water oxidation · X-ray diffraction

[1] a) H. Yoo, Y.-W. Choi, J. Choi, *ChemCatChem* **2015**, *7*, 643 – 647; b) M. Rodríguez, I. Romero, C. Sens, A. Llobet, *J. Mol. Catal. A* **2006**, *251*, 215 – 220.

[2] a) S. Cherevko, T. Reier, A. R. Zeradjanin, Z. Pawolek, P. Strasser, K. J. J. Mayrhofer, *Electrochem. Commun.* **2014**, *48*, 81 – 85; b) A. Minguzzi, C. Locatelli, O. Lugaresi, E. Achilli, G. Cappelletti, M. Scavini, M. Coduri, P. Masala, B. Sacchi, A. Vertova, P. Ghigna, S. Rondinini, *ACS Catal.* **2015**, *5*, 5104 – 5115; c) J. C. Hidalgo-Acosta, M. A. Méndez, M. D. Scanlon, H. Vrubel, V. Amstutz, W. Adamiak, M. Opallo, H. H. Girault, *Chem. Sci.* **2015**, *6*, 1761 – 1769.

[3] a) G. Mattioli, P. Giannozzi, A. A. Bonapasta, L. Guidoni, *J. Am. Chem. Soc.* **2013**, *135*, 15353 – 15363; b) M. Zhang, M. D. Respinis, H. Frei, *Nat. Chem.* **2014**, *6*, 362 – 367; c) D. Wang, J. T. Groves, *Proc. Natl. Acad. Sci. USA* **2013**, *110*, 15579 – 15584; d) B. Das, A. Orthaber, S. Ott, A. Thapper, *Chem. Commun.* **2015**, *51*, 13074 – 13077; e) A. I. Nguyen, M. S. Ziegler, P. Oña-Burgos, M. Sturzbecher-Hohne, W. Kim, D. E. Bellone, T. D. Tilley, *J. Am. Chem. Soc.* **2015**, *137*, 12865 – 12872.

[4] a) M. Hatakeyama, H. Nakata, M. Wakabayashi, S. Yokojima, S. Nakamura, *J. Phys. Chem. A* **2012**, *116*, 7089 – 7097; b) K. Jin, J. Park, J. Lee, K. D. Yang, G. K. Pradhan, U. Sim, D. Jeong, H. L. Jang, S. Park, D. Kim, N.-E. Sung, S. H. Kim, S. Han, K. T. Nam, *J. Am. Chem. Soc.* **2014**, *136*, 7435 – 7443; c) A. Han, H. Chen, Z. Sun, J. Xu, P. Du, *Chem. Commun.* **2015**, *51*, 11626 – 11629; d) R. Brimblecombe, D. R. J. Kolling, A. M. Bond, G. C. Dismukes, G. F. Swiegers, L. Spiccia, *Inorg. Chem.* **2009**, *48*, 7269 – 7279.

[5] a) Y. Han, Y. Wu, W. Lai, R. Cao, *Inorg. Chem.* **2015**, *54*, 5604 – 5613; b) L. Wang, L. Duan, R. B. Ambre, Q. Daniel, H. Chen, J. Sun, B. Das, A. Thapper, J. Uhlig, P. Dinér, L. Sun, *J. Catal.* **2016**, *335*, 72 – 78; c) M. Zhang, M.-T. Zhang, C. Hou, Z.-F. Ke, T.-B. Lu, *Angew. Chem. Int. Ed.* **2014**, *53*, 13042 – 13048; *Angew. Chem.* **2014**, *126*, 13258 – 13264.

[6] a) J. J. H. Pijpers, M. T. Winkler, Y. Surendranath, T. Buonassisi, D. G. Nocera, *Proc. Natl. Acad. Sci. USA* **2011**, *108*, 10056 – 10061; b) H. S. Ahn, A. J. Bard, *J. Am. Chem. Soc.* **2015**, *137*, 612 – 615; c) S. K. Pilli, T. E. Furtak, L. D. Brown, T. G. Deutsch, J. A. Turnerc, A. M. Herring, *Energy Environ. Sci.* **2011**, *4*, 5028 – 5034.

[7] a) X.-B. Han, Z.-M. Zhang, T. Zhang, Y.-G. Li, W. Lin, W. You, Z.-M. Su, E.-B. Wang, *J. Am. Chem. Soc.* **2014**, *136*, 5359 – 5366; b) J. Soriano-López, S. Goberna-Ferrón, L. Vigara, J. J. Carbó, J. M. Poblet, J. R. Galán-Mascarós, *Inorg. Chem.* **2013**, *52*, 4753 – 4755; c) J. J. Stracke, R. G. Finke, *J. Am. Chem. Soc.* **2011**, *133*, 14872 – 14875.

[8] D. Wang, G. Ghirlanda, J. P. Allen, *J. Am. Chem. Soc.* **2014**, *136*, 10198 – 10201.

[9] B. J. Deibert, J. Zhang, P. F. Smith, K. W. Chapman, S. Rangan, D. Banerjee, K. Tan, H. Wang, N. Pasquale, F. Chen, K.-B. Lee, G. C. Dismukes, Y. J. Chabal, J. Li, *Chem. Eur. J.* **2015**, *21*, 14218 – 14228.

[10] R. L. Lieberman, D. B. Shrestha, P. E. Doan, B. M. Hoffman, T. L. Stemmler, A. C. Rosenzweig, *Proc. Natl. Acad. Sci. USA* **2003**, *100*, 3820 – 3825.

[11] D. Horn, A. Barrientos, *IUBMB Life* **2008**, *60*, 421 – 429.

[12] S. M. Barnett, K. I. Goldberg, J. M. Mayer, *Nat. Chem.* **2012**, *4*, 498 – 502.

[13] Z. Chen, T. J. Meyer, *Angew. Chem. Int. Ed.* **2013**, *52*, 700 – 703; *Angew. Chem.* **2013**, *125*, 728 – 731.

[14] J. S. Pap, Ł. Szyrwiel, D. Srankó, Z. Kerner, B. Setner, Z. Szewczuk, W. Malink, *Chem. Commun.* **2015**, *51*, 6322 – 6324.

[15] a) C. Lu, J. Wang, Z. Chen, *ChemCatChem* **2016**, *8*, 2165 – 2170; b) X. Liu, S. Cui, M. Qian, Z. Sun, P. Du, *Chem. Commun.* **2016**, *52*, 5546 – 5549.

[16] T. Zhang, C. Wang, S. Liu, J.-L. Wang, W. Lin, *J. Am. Chem. Soc.* **2014**, *136*, 273 – 281.

[17] X. Liu, S. Cui, Z. Sun, Y. Ren, X. Zhang, P. Du, *J. Phys. Chem. C* **2016**, *120*, 831 – 840.

[18] a) B. Shankar, P. Elumalai, R. Shanmugam, V. Singh, D. T. Masram, M. Sathiyendiran, *Inorg. Chem.* **2013**, *52*, 10217 – 10219; b) A.-F. Shihada, F. Weller, *Z. Naturforsch. B* **1996**, *51*, 1111 – 1116; c) J. Beckmann, D. Dakternieks, A. Duthie, C. Mitchell, F. Ribot, J. B. d'Espinose de la Caillerie, B. Revel, *Appl. Organomet. Chem.* **2004**, *18*, 353 – 358; d) M. Hatano, E. Takagi, K. Ishihara, *Org. Lett.* **2007**, *9*, 4527 – 4530; e) Y. Hasegawa, R. Hieda, T. Nakagawa, T. Kawai, *Helv. Chim. Acta* **2009**, *92*, 2238 – 2248; f) D. Rosario-Amorin, S. Ouizem, D. A. Dickie, R. T. Paine, R. E. Cramer, B. P. Hay, J. Podair, L. H. Delmau, *Inorg. Chem.* **2014**, *53*, 5698 – 5711.

[19] a) Y. Yan, M. Juríček, F.-X. Coudert, N. A. Vermeulen, S. Grunder, A. Dailly, W. Lewis, A. J. Blake, J. F. Stoddart, M. Schröder, *J. Am. Chem. Soc.* **2016**, *138*, 3371 – 3381; b) C.-S. Liu, J.-J. Wang, l.-F. Yan, Z. Chang, X.-H. Bu, E. C. Sañudo, J. Ribas, *Inorg. Chem.* **2007**, *46*, 6299 – 6310.

[20] K. Takahashi, N. Hoshino, T. Takeda, S.-I. Noro, T. Nakamura, S. Takeda, T. Akutagawa, *Inorg. Chem.* **2015**, *54*, 9423 – 9431.

[21] F. P. W. Agterberg, H. A. J. Provó Kluit, W. L. Driessen, H. Oevering, W. Buijs, M. T. Lakin, A. L. Spek, J. Reedijk, *Inorg. Chem.* **1997**, *36*, 4321 – 4328.

[22] Y. Zhao, D.-S. Deng, L.-F. Ma, B.-M. Jib, L.-Y. Wang, *Chem. Commun.* **2013**, *49*, 10299 – 10301.

[23] J. B. Gerken, J. G. McAlpin, J. Y. C. Chen, M. L. Rigsby, W. H. Casey, R. D. Britt, S. S. Stahl, *J. Am. Chem. Soc.* **2011**, *133*, 14431 – 14442.

[24] J. Du, Z. Chen, S. Ye, B. J. Wiley, T. J. Meyer, *Angew. Chem. Int. Ed.* **2015**, *54*, 2073 – 2078; *Angew. Chem.* **2015**, *127*, 2101 – 2106.

[25] F. Yu, F. Li, B. Zhang, H. Li, L. Sun, *ACS Catal.* **2015**, *5*, 627 – 630.

[26] X. Liu, H. Zheng, Z. Sun, A. Han, P. Du, *ACS Catal.* **2015**, *5*, 1530 – 1538.

[27] T.-T. Li, S. Cao, C. Yang, Y. Chen, X.-J. Lv, W.-F. Fu, *Inorg. Chem.* **2015**, *54*, 3061 – 3067.

[28] a) A. S. Duke, E. A. Dolgopolova, R. P. Galhenage, S. C. Ammal, A. Heyden, M. D. Smith, D. A. Chen, N. B. Shustova, *J. Phys. Chem. C* **2015**, *119*, 27457 – 27466; b) D. Deng, T. Qi, Y. Cheng, Y. Jin, F. Xiao, *J. Mater. Sci. Mater. Electron.* **2014**, *25*, 390 – 397.

[29] S.-M. Chang, C.-Y. Hou, P.-H. Lo, C.-T. Chang, *Appl. Catal. B* **2009**, *90*, 233 – 241.

[30] a) J. Morales, L. Sánchez, F. Martín, J. R. Ramos-Barrado, M. Sánchez, *Electrochim. Acta* **2004**, *49*, 4589 – 4597; b) C. D. Wagner, W. M. Riggs, L. E. Davis, J. F. Moulder in *Handbook of X-ray Photoelectron Spectroscopy: A Reference Book of Standard Data for Use in X-ray Photoelectron Spectroscopy* (Ed.: G. E. Muilenberg), PerkinElmer Corp., Physical Electronics Division, Eden Prairie, MN, **1979**, p. 82.

[31] E. Cano, C. L. Torres, J. M. Bastidas, *Mater. Corros.* **2001**, *52*, 667 – 676.

[32] Y. Chen, W. Liu, C. Ye, L. Yu, S. Qi, *Mater. Res. Bull.* **2001**, *36*, 2605 – 2612.

[33] B. K. Park, S. Jeong, D. Kim, J. Moon, S. Lim, J. S. Kim, *J. Colloid Interface Sci.* **2007**, *311*, 417 – 424.

[34] K. Asami, K. Hashimoto, S. Shimodaira, *Corros. Sci.* **1978**, *18*, 151 – 160.

[35] K. S. Joya, H. J. M. de Groot, *ACS Catal.* **2016**, *6*, 1768 – 1771.

[36] International Tables for X-Ray Crystallography, Kynoch Press, Vol. III, Birmingham, UK, **1952**.

[37] SAINT, version 6.02, Bruker AXS, Madison, WI, **1999**.

[38] G. M. Sheldrick, SADABS, Empirical Absorption Correction Program; University of Göttingen: Göttingen, Germany, **1997**.

[39] XPREP, version 5.1; Siemens Industrial Automation Inc., Madison, WI, **1995**.

[40] G. M. Sheldrick, SHELXTL Reference Manual, version 5.1, Bruker AXS: Madison, WI, **1997**.

[41] G. M. Sheldrick, SHELXL-97: Program for Crystal Structure Refinement; University of Göttingen, Göttingen, Germany, **1997**.

Manuscript received: August 26, 2016
Accepted Article published: September 12, 2016
Final Article published: September 28, 2016